

Provided for non-commercial research and education use.
Not for reproduction, distribution or commercial use.



This article appeared in a journal published by Elsevier. The attached copy is furnished to the author for internal non-commercial research and education use, including for instruction at the authors institution and sharing with colleagues.

Other uses, including reproduction and distribution, or selling or licensing copies, or posting to personal, institutional or third party websites are prohibited.

In most cases authors are permitted to post their version of the article (e.g. in Word or Tex form) to their personal website or institutional repository. Authors requiring further information regarding Elsevier's archiving and manuscript policies are encouraged to visit:

<http://www.elsevier.com/copyright>



ELSEVIER

Journal of Environmental Management 90 (2009) 2219–2225

 Journal of
**Environmental
 Management**

www.elsevier.com/locate/jenvman

Predictive models of turbidity and water depth in the Doñana marshes using Landsat TM and ETM+ images

Javier Bustamante^{a,b,*}, Fernando Pacios^{a,b}, Ricardo Díaz-Delgado^{a,b}, David Aragonés^{a,b}

^a Laboratorio de Sig y Teledetección (LAST-EBD), Estación Biológica de Doñana, CSIC, Avda. María Luisa s/n, 41013 Sevilla, Spain

^b Departamento de Ecología Integrativa, Estación Biológica de Doñana, CSIC, Avda. María Luisa s/n, 41013 Sevilla, Spain

Received 20 October 2006; received in revised form 27 July 2007; accepted 2 August 2007

Available online 18 April 2008

Abstract

We have used Landsat-5 TM and Landsat-7 ETM+ images together with simultaneous ground-truth data at sample points in the Doñana marshes to predict water turbidity and depth from band reflectance using Generalized Additive Models. We have point samples for 12 different dates simultaneous with 7 Landsat-5 and 5 Landsat-7 overpasses. The best model for water turbidity in the marsh explained 38% of variance in ground-truth data and included as predictors band 3 (630–690 nm), band 5 (1550–1750 nm) and the ratio between bands 1 (450–520 nm) and 4 (760–900 nm). Water turbidity is easier to predict for water bodies like the Guadalquivir River and artificial ponds that are deep and not affected by bottom soil reflectance and aquatic vegetation. For the latter, a simple model using band 3 reflectance explains 78.6% of the variance. Water depth is easier to predict than turbidity. The best model for water depth in the marsh explains 78% of the variance and includes as predictors band 1, band 5, the ratio between band 2 (520–600 nm) and band 4, and bottom soil reflectance in band 4 in September, when the marsh is dry. The water turbidity and water depth models have been developed in order to reconstruct historical changes in Doñana wetlands during the last 30 years using the Landsat satellite images time series.

© 2008 Elsevier Ltd. All rights reserved.

Keywords: Water turbidity; Water depth; Marshland; Remote sensing; Wetlands; GAM; GLM

1. Introduction

Doñana marshes constitute a vast seasonal freshwater wetland of international importance. They are Europe's largest sanctuary for migrating birds. They were declared National park in 1969, Biosphere reserve in 1980, Important Wetland Site under the Ramsar Convention in 1982 and Natural World Heritage Site in 1984 (García Novo and Marín Cabrera, 2006). The variable winter rains flood Doñana marshes forming a wide shallow lake that dries up during spring and summer. Flooded areas are very variable in depth and turbidity, and they change depending on the amount and pattern of rainfall and time of the year. In order to study the historical dynamics of Doñana

wetlands during the last 30 years, we acquired a time series of Landsat Multi Spectral Scanner (MSS), Thematic Mapper (TM) and Enhanced Thematic Mapper (ETM+) images.

Satellite images from multispectral sensors have been used to map flooded areas or to derive characteristics of the water mass like turbidity, water depth, phytoplankton biomass, or aquatic vegetation cover. Most studies have focused on one or few parameters, in the sea or deep inland waters, and little is known if the same models can be successfully applied to shallow heterogeneous wetlands in which some factors may interfere in the estimation of others.

We are interested in developing and testing an empirical model to predict water turbidity and water depth in shallow waters of the Doñana marshes that can be used to predict water turbidity and depth in historical satellite multispectral images. Some preliminary models of water turbidity and depth with data for two Landsat-5 images have already been published (Bustamante et al., 2005).

* Corresponding author. Laboratorio de Sig y Teledetección (LAST-EBD), Estación Biológica de Doñana, CSIC, Avda. María Luisa s/n, 41013 Sevilla, Spain. Tel.: +34 954 232340; fax: +34 954 621125.

E-mail address: jbstamante@ebd.csic.es (J. Bustamante).

2. Material and methods

2.1. Sampling campaigns

We performed two different field sampling campaigns. The first one (called hereafter *river*) was directed to build a water turbidity model for inland waters not severely affected by aquatic vegetation and bottom soil reflectance. For this purpose we sampled water turbidity at 12 fixed points on the Guadalquivir River, Guadalquivir River port, gravel extraction ponds and irrigation reservoirs. These areas usually show a gradient in water turbidity in a single date going from low turbidity in irrigation reservoirs to high or very high turbidity in the Guadalquivir River. The second sampling (called hereafter *marsh*) was directed to build a turbidity and water depth model in the shallow heterogeneous marshland, with water depth ranging from 5 to 200 cm, and a variable degree of aquatic vegetation cover. We performed linear transects on foot in marsh flooded areas taking point samples at least 60 m apart. At each sampling point we measured turbidity, water depth and aquatic vegetation cover. We performed 12 *river* sampling campaigns and 14 *marsh* sampling campaigns close to programmed Landsat-5 (TM) and Landsat-7 (ETM+) overpasses between 4 December 2003 and 10 April 2006. Field work resulted in 7 *river* and 7 *marsh* campaigns less than 5 days from 12 satellite cloudless images (7 Landsat-5 TM images and 5 Landsat-7 ETM+ images).

2.2. Field measurements

Sample points were positioned with a navigation GPS with 5–15 m precision. Turbidity was measured in NTU with a nephelometric turbidimeter (Hanna Instruments mod. HI 93703). We took three water samples at each *river* sampling point, measured turbidity *in situ*, and calculated the mean turbidity. In the *marsh* we took a single sample at each point and measured turbidity *in situ* or within 24 h of taking the sample. Water depth was measured at the sample point in centimetres with a measuring rod with 1-cm precision. Aquatic vegetation cover was estimated by eye in a circle of 15-m diameter around the sample point in four categories (absent, <25% cover, 25–75% cover, >75% cover), distinguishing among submerged, floating and emergent vegetation and whether it was green or dry.

2.3. Image processing

A Landsat-7 ETM+ reference image from 18 July 2002 was georeferenced with 100 control points using aerial orthophotos of the Junta de Andalucía (2003). The remaining satellite images were co-registered to this reference image. The resampling method was cubic convolution. Mean ground error calculated with independent test point on co-registered images was 19.7 m. Images were first radiometrically corrected and transformed into reflectance values using Pons and Solé-Sugrañes (1994) method implemented in MIRAMON based on a dark object model. Images were then normalized using

a set of pseudo-invariant areas comprising over 60,000 pixels, covering all the range of reflectance values, and selected from eight area types: deep sea, reservoirs, sand dunes, rocky outcrops, bare soils, airport runways, urban areas and open mines, that were expected to have low seasonal changes in reflectance. We calculated a cloud mask and pseudo-invariant pixels were rejected if covered by clouds. We took as reference image the Landsat-7 ETM+ of 18 July 2002 and calculated a linear regression using all potential pseudo-invariant pixels. All pixels with residuals greater than 1 S.D. were assumed to have significant changes in reflectance and rejected, and a new regression line was calculated. The offset and gain from this regression were used to normalize the reflectance values of the satellite image.

In the *river* data set the water at each sample point was relatively homogeneous in turbidity, so we extracted the mean radiometric values for a flooded area surrounding the sample point of approximately 11 pixels (9900 m²) or the whole flooded area for small ponds. This area was delineated on each image to correct for differences in flooded surface. Water depth and turbidity in the *marsh* changed gradually and was spatially heterogeneous; so for each sample point we extracted radiometric data from the single pixel overlapping the sample point. In the *river* data set we ended with 53 valid samples with turbidity and radiometric data, while in the *marsh* data set we ended with 220 points in flooded areas that had turbidity, water depth and radiometric data.

2.4. Empirical models

We initially fitted Generalized Additive Models (GAM, Hastie and Tishirani, 1990) to the response variables water turbidity (in NTU) and depth (in cm) that were log transformed (natural logarithms), using normal errors and an identity link. As potential predictors we used the normalized reflectance of TM or ETM+ bands (B) 1, 2, 3, 4, 5 and 7 and ratios between bands B1/B2, B2/B3, B3/B4 and VIS/NIR = (B1 + B2 + B3)/B4. As we expected that differences in bottom soil reflectance could interfere with turbidity and depth estimation, in *marsh* data we also tested as covariables: bottom soil reflectance when the marsh was dry (reflectance from an image in September), and the ratio between reflectance on sampling date and reflectance in September for each band. In the case of turbidity we also tested depth as a covariate, and in the case of depth we also tested the difference between reflectance in the date and reflectance in September for each band. Turbidity models were built for *river* and *marsh* data while depth models were only built for *marsh* data.

We fitted models with a forward–backward predictor selection procedure, the STEP GAM procedure in S-Plus (Mathsoft Inc., 1999), starting from a null model and using smooth splines with up to three degrees of freedom for the relation between the predictor and the response variable. Only variables that significantly increased explained variance ($p < 0.01$) with an F -test were retained in the model. The partial response graphs of the predictors included in the model were explored and piece-wise Generalized Linear Models (GLM,

MacCullagh and Nelder, 1989) were tested for those predictors that the automatic procedure had selected a smooth spline. If the piece-wise linear models were not significantly different, these were preferred because they are easier to interpret and to implement in a GIS.

3. Results

3.1. Turbidity

The best model selected with the step-wise procedure with the *river* data included only B3 (630–690 nm) and indicated a linear positive correlation between turbidity and B3 reflectance, explaining 78.6% of the variance (Fig. 1). Even though the graph might suggest an important effect of three outlier samples in the regression (three very turbid river samples after a flood), the model does not change significantly after excluding those three samples ($F = 1.16$, $P = 0.333$).

The best GAM model selected with the step-wise procedure with the *marsh* data included B3, B5 and the ratio B1/B4, and indicated positive curvilinear relationship with B3, a negative curvilinear relationship with B5 and a negative linear relationship with the ratio B1/B4 (Fig. 2). The model explained 40% of variance in turbidity. Neither water depth nor the variables indicating bottom soil reflectance could improve this model. This model was transformed into a piece-wise linear model by making constant the additive effect of B3 for reflectances >0.2 and of B5 for reflectances >0.09 (Fig. 3). This was a simple relationship suggested by the partial effects in Fig. 2. This model explained 37.69% of the variance in turbidity. The increase in unexplained variance was only marginally significant when compared with the GAM model ($F = 2.76$, $P = 0.043$).

We also compared our empirical models with the Water Turbidity Index ($WTI = 0.91B3 + 0.43B4$) suggested by Yamagata et al. (1988) for TM images. The WTI was significantly correlated with water turbidity measured in the field ($r = 0.90$, Student's $t = 14.66$, $df = 51$, one-tailed $p < 0.001$ for *river* data, $r = 0.17$, $t = 2.629$, $df = 218$, one-tailed $p = 0.005$ for *marsh* data). The WTI explained 75% of the variance in *river* data and 14% of the variance for *marsh* data. In

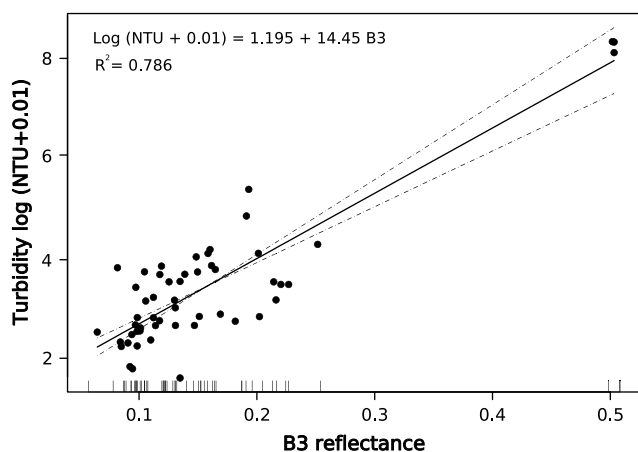


Fig. 1. Best step-wise model GAM for water turbidity with *river* data.

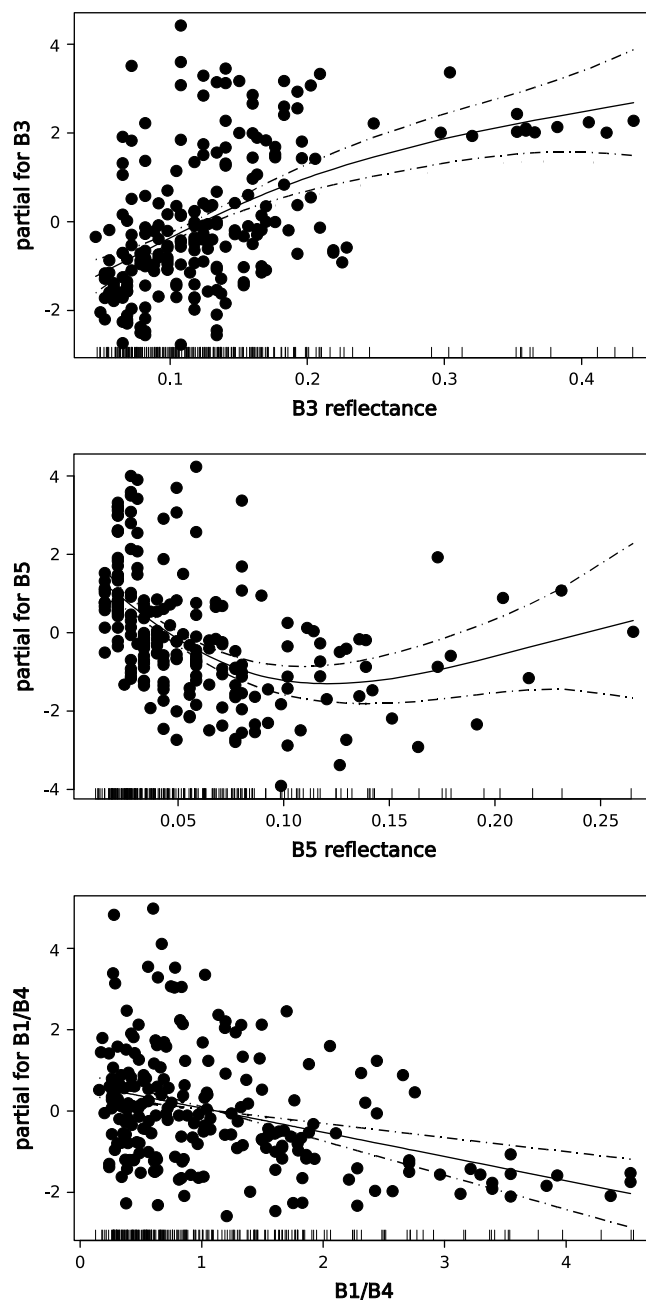


Fig. 2. Partial additive effects (continuous line) and its standard error (discontinuous line) of the best step-wise GAM model for water turbidity in the marsh.

both cases the WTI was a significantly worse predictor than our models.

3.2. Water depth

The best model selected with the step-wise procedure with the *marsh* data included the B1, B5, B2/B4, bottom soil reflectance in B4 (from an image in September, when the marsh is completely dry) and the ratio between reflectance in the date and reflectance in September in B4 (Fig. 4). The model explained 75.42% of the variance. The GAM model could be

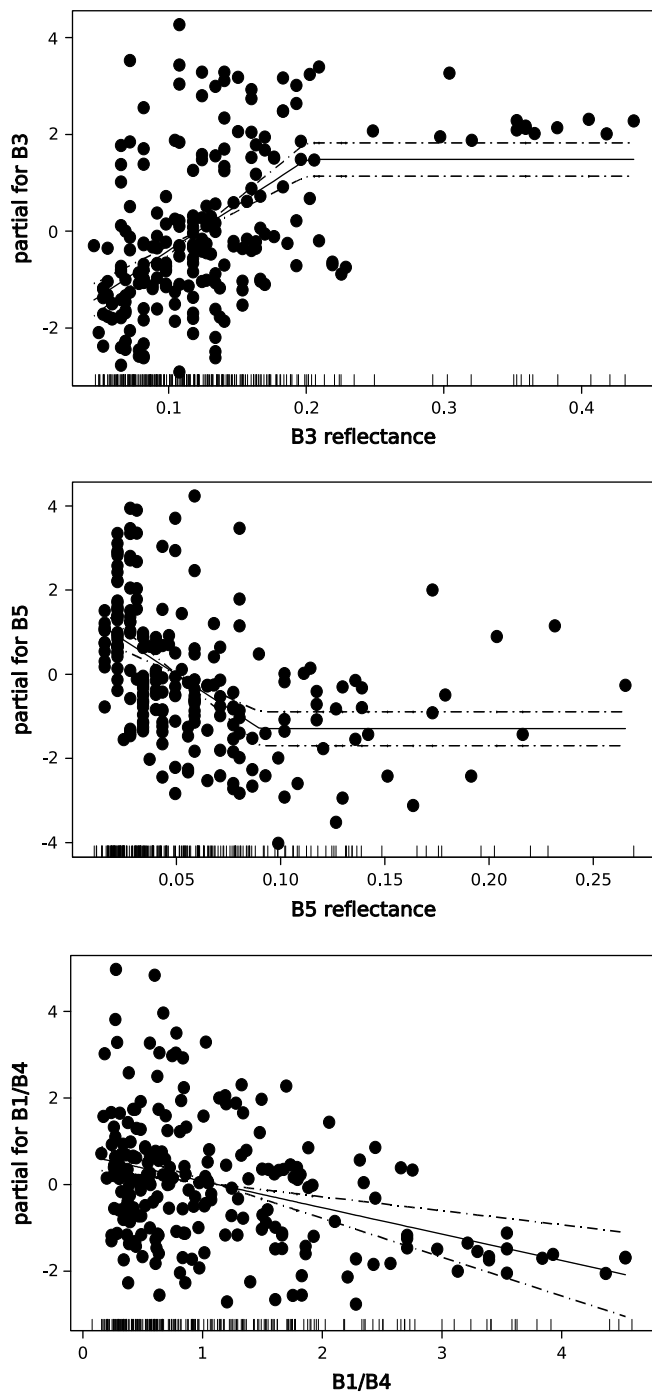


Fig. 3. Partial additive effects and S.E. of the piece-wise linear model for water turbidity in the marsh derived from the step-wise GAM model.

transformed into a piece-wise linear GLM by assuming a constant additive effect of B1 for reflectance >0.1 and for B1/B4 >2.5 (Fig. 5). This model explained 78.2% of the variance in depth, slightly more than the GAM model.

4. Discussion

Our results show that it is possible to build empirical models to estimate water turbidity and water depth from

reflectance data from TM or ETM+ Landsat sensors. Water turbidity is better estimated in situations in which bottom soil reflectance and aquatic vegetation do not interfere, but it is still possible to build a predictive model for situations like those of the Doñana marshes with shallow waters and abundant aquatic vegetation (Fig. 6). In those situations it is possible to distinguish between clear and turbid water; but there is an important amount of variance not explained by the model, and an accurate estimate of turbidity values is not possible. The water turbidity model for the *river* data is a simple model in which turbidity shows a linear relation with reflectance in B3 (the red region of the spectrum). Suspended sediments in water increase the reflectance in the red portion of the spectrum and they are probably the main cause of turbidity in *river* data. The water turbidity index (WTI) proposed by Yamagata et al. (1988) has a similar behavior to our model for *river* data, but is slightly more complex (requires two spectral bands, B3 and B4, instead of one) and does not explain more variance. The water turbidity model for the *marsh* shows also a positive relationship with B3, but is necessary to include more bands to correct for the effect of bottom soil reflectance and aquatic vegetation. Photosynthetically active aquatic vegetation absorbs in the red portion of the spectrum while suspended sediments reflect in this portion of the spectrum. In this situation it is clear that our empirical model works much better than the WTI and explains twice as much variance in field data. The results suggest that although TM or ETM+ B3 reflectance of flooded areas can be used as a proxy for water turbidity, better results can be obtained by fitting an empirical model that is specific for situations with shallow waters and aquatic vegetation.

Airborne LIDAR bathymetry (ALB) is an active optical system that has been used to reconstruct depth in coastal waters in the range from 1.5 to 60 m (Guenther et al., 2000; Wang and Philpot, 2007). Current ALB systems have a limited vertical accuracy around 0.25 m (Baltasvias, 1999), which limits their operational use in shallow wetlands. They have not been tested in shallow wetlands as far as we know. Our results show that it is possible to estimate water depth in the Doñana marshes' with reflectance data from TM and ETM+ sensors (Fig. 7) and the resulting models have relatively good accuracy, greater accuracy than those for water turbidity. Our results indicate that it is important to take into account differences in bottom soil reflectance. In the case of Doñana this is possible because the marshland dries up during summer. The results suggest the feasibility of studying historical changes in water depth with Landsat reflectance data, something that cannot be done with an ALB system, and so try to reconstruct the recent dynamics in the process of marsh siltation.

5. Conclusions

- Predictive models allow water turbidity and water depth mapping from Landsat TM or ETM+ images in shallow wetlands such as Doñana marshes.

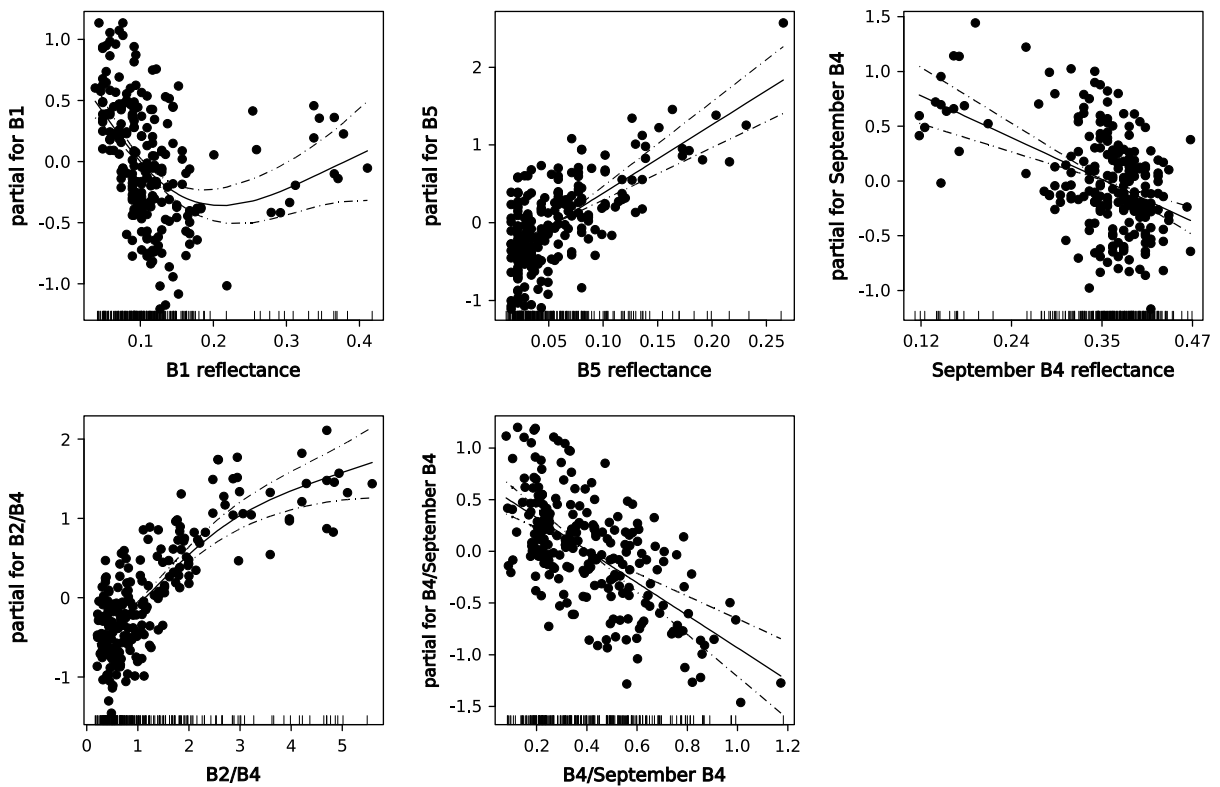


Fig. 4. Partial additive effects and S.E. of the best step-wise GAM model for water depth in the marsh.

- Overall accuracy is much better for water depth models than for water turbidity models but both allow accurate enough historical reconstruction of turbidity and depth patterns across the area of Doñana marshes (Díaz-Delgado et al., 2006).
- Reconstruction of water turbidity regimes from the available time series of Landsat images is aiding to understand main trends of siltation processes inside Doñana marshes as well as changes in aquatic plant cover.

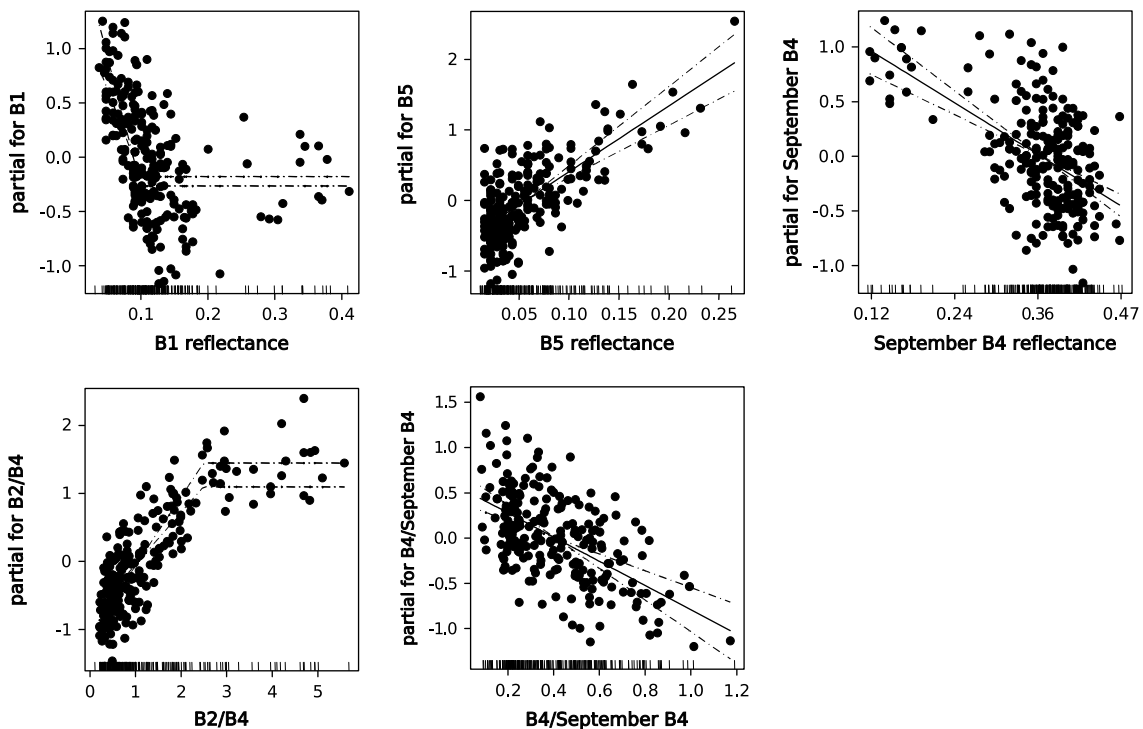


Fig. 5. Partial additive effects and S.E. of the piece-wise linear model for water depth in the marsh derived from the GAM model.

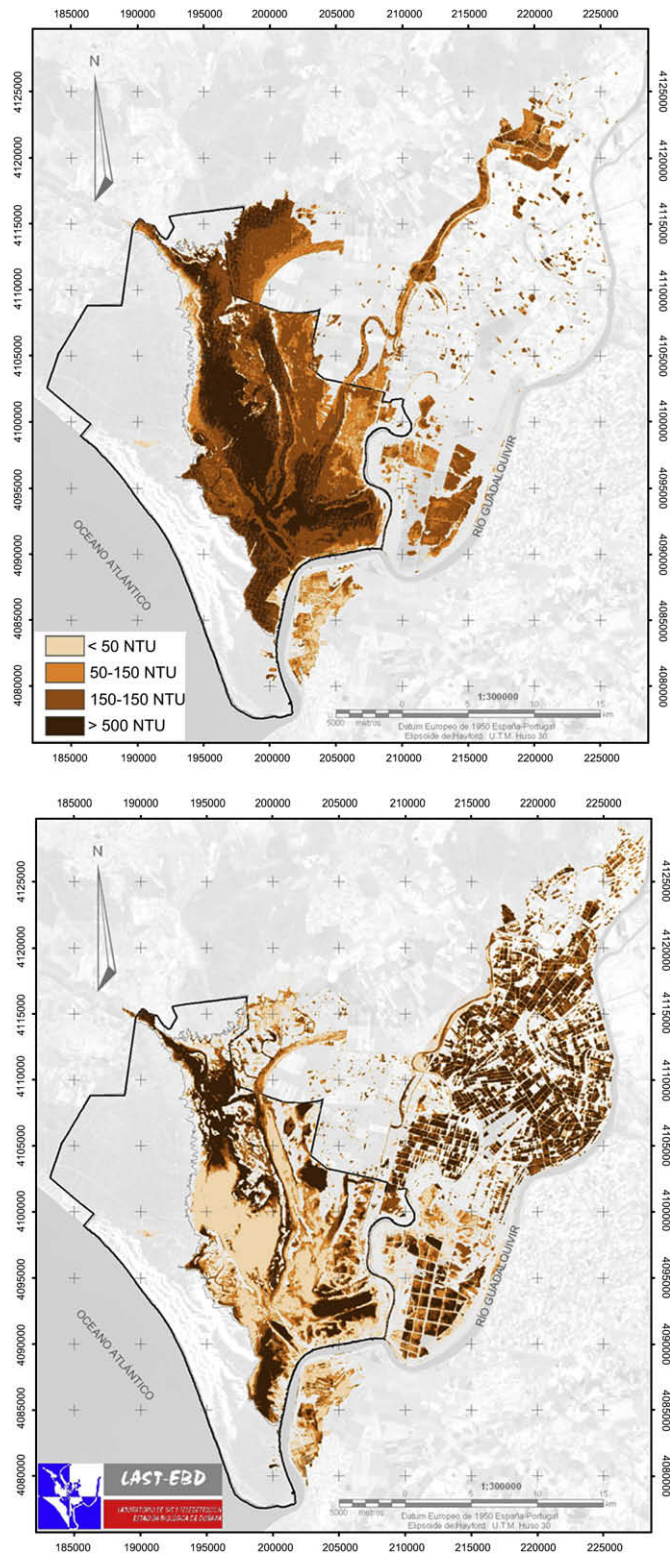


Fig. 6. Reclassified water turbidity maps of the Doñana marshes resulting from the application of the piece-wise linear model for *marsh* data. Upper map is the situation on 14 January 1990. Lower map is the situation on 10 January 2003.

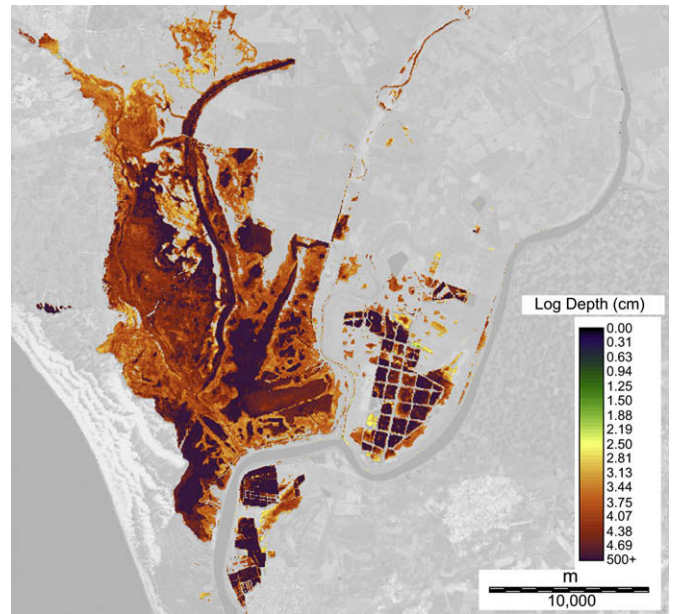


Fig. 7. Water depth map of flooded area in the Doñana marshes in logarithmic scale. Result from the application of the piece-wise linear model to an image from 25 March 2004.

Acknowledgements

This study was funded by Doñana National Park administration (Spanish Ministry of Environment) through the research project “Reconstruction of bird population dynamics during the last three decades” and by the Spanish Ministry of Science and Education through the research project HYDRA (# CGL2006-02247/BOS) and help from the National Environmental Remote Sensing Network (# CGL2007-28828-E/BOS). F. Pacios was funded by an I3P fellowship from the CSIC. Doñana National Park and Natural Park provided permits for field work in protected areas with restricted access. A. Travaini, H. Le Franc, D. Paz, A. Polvorinos, and I. Román helped with field work. J.C. Gilabert, J.L. Pecharromán and P.L. Porta helped with image processing.

References

Baltsavias, E.P., 1999. Airborne laser scanning: existing systems and firms and other resources. *ISPRS Journal of Photogrammetry & Remote Sensing* 54, 164–198.

Bustamante, J., Díaz-Delgado, R., Aragonés, D., 2005. Determinación de las características de aguas someras en las marismas de Doñana mediante teledetección. *Revista de Teledetección* 24, 107–111.

Díaz-Delgado, R., Bustamante, J., Aragonés, D., Pacios, F., 2006. Determining water body characteristics of Doñana shallow marshes through remote sensing. In: *IEEE International Conference on Geoscience and Remote Sensing Symposium*, 2006, July 31 2006–August 4 2006, IGARSS 2006, pp. 3662–3663, doi:10.1109/IGARSS.2006.938.

García Novo, F., Marín Cabrera, C., 2006. Doñana: Agua y Biosfera. Doñana 2005. Confederación Hidrográfica del Guadalquivir, Ministerio de Medio Ambiente, Madrid.

Guenther, G.C., Cunningham, A.G., LaRocque, P.E., Reid, D.J., 2000. Meeting the accuracy challenge in airborne LIDAR bathymetry. In: *Proceedings of the 20th EARSeL Symposium: Workshop on LIDAR Remote Sensing of Land and Sea*, June 16–17, Dresden, Germany. European Association of Remote Sensing Laboratories (paper #1 on CD), 23 pp.

- Hastie, T.J., Tishirani, R.J., 1990. *Generalized Additive Models*. Chapman & Hall, London.
- Junta de Andalucía, 2003. *Ortofotografía digital de Andalucía (Color)*. Color Photogrammetric flight 1:60,000 (1998–1999). Junta de Andalucía.
- MacCullagh, P., Nelder, J.A., 1989. *Generalized Linear Modelling*, second ed.). Chapman & Hall, London.
- Mathsoft Inc., 1999. *S-Plus User Guide*. Data Analysis. Products Division, Mathsoft Inc., Seattle.
- Pons, X., Solé-Sugrañes, L., 1994. A simple radiometric correction model to improve automatic mapping of vegetation from multispectral satellite data. *Remote Sensing of Environment* 48, 191–204.
- Wang, Ch-K., Philpot, W.D., 2007. Using airborne bathymetric LIDAR to detect bottom type variation in shallow waters. *Remote Sensing of Environment* 106, 123–135.
- Yamagata, Y., Wiegand, C., Akiyama, T., Shibayama, M., 1988. *Remote Sensing of Environment* 26, 241–251.